An Infrared and X-ray Absorption Study of the Equilibria and Structures of Chromate, Bichromate, and Dichromate in Ambient Aqueous Solutions

Markus M. Hoffmann,[†,§] John G. Darab,[‡] and John L. Fulton*[,†]

Fundamental Sciences Division, and Energy Science & Technology Division, Pacific Northwest National Laboratory, Richland, Washington 99352

Received: July 31, 2000

The structure and equilibrium of chromate (CrO_4^{2-}), bichromate ($HCrO_4^-$), and dichromate ($Cr_2O_7^{2-}$) in ambient aqueous solutions was investigated by both IR and X-ray absorption fine structure (XAFS) spectroscopy. The individual IR bands for each of these species have been identified, and quantitative analysis of the IR bands was used to examine the chemical equilibria. A dilution study at a constant, low solution pH revealed the speciation change from dichromate dominance at high total chrome concentration to bichromate dominance at low total chrome concentration, thereby unequivocally confirming the existence of the bichromate species. The equilibrium constants, obtained from the quantitative analysis of the IR data, agree well with previously reported values. The quantitative IR analysis also revealed that the asymmetric $\nu_{as}(CrO_3)$ stretching frequency is virtually coincident for the bi- and dichromate. The complete structural analysis of chromate, bichromate, and dichromate was obtained from an XAFS study of chromate solutions of varying total chrome concentration. The XAFS results confirm the $\nu_{as}(CrO_3)$ IR band assignment for both the bi- and dichromate species by showing that the first-shell structure around the central chrome atom is nearly identical for the bi-and dichromate molecular ions. Within experimental uncertainty, the Cr−O bond distance that is associated with the $\nu_{as}(CrO_3)$ vibrational mode was found to be identical for the bi- and dichromate structures.

Introduction

The chemistry present in aqueous chromate solutions described by the following chemical equilibria is well established.[1−6]

$$CrO_4^{2-} + H^+ \rightleftharpoons HCrO_4^- \quad (1)$$

$$2CrO_4^{2-} + 2H^+ \rightleftharpoons Cr_2O_7^{2-} + H_2O \quad (2)$$

$$2HCrO_4^- \rightleftharpoons Cr_2O_7^{2-} + H_2O \quad (3)$$

In particular, most of the early investigations, such as the ones cited by Sasaki,[2] employed indirect measurements such as conductivity, calorimetry, and electromotive force measurements to infer the existence of the individual chromate, bichromate, and dichromate species. Other spectroscopic investigations include UV−vis[7,8] and Raman measurements.[9−11] In sharp contrast to this large body of experimental observations, the Raman investigations by Michel and co-workers questioned the existence of the bichromate species due to the absence of this species's predicted $\nu_s(CrO_3)$ symmetric stretching mode.[9,10] As pointed out by this group, this Raman-active band has been observed for the analogous chemical species HSO_4^- and $HSeO_4^-$.[12,13] The subsequent Raman investigation conducted by Palmer et al., at temperatures up to 245 °C where the bichromate species is predicted to be dominant, also did not reveal a distinctive bichromate band, and these authors suggested that the Raman-active symmetric stretching mode $\nu_s(CrO_3)$ of bichromate may be coincident with the $\nu_s(CrO_3)$ mode of dichromate.[11] One objective of this paper is, then, to resolve this discrepancy by investigating the corresponding IR-active vibrational modes of the various chromate equilibrium species. To the best of our knowledge, IR spectroscopic data for the aqueous chromate system have not been previously reported; this is presumably because very short optical path lengths are required for data collection due to the high IR absorbency of water. A second objective is to use XAFS spectroscopy to obtain detailed structural information (bond distances, bond angles, and bond strengths, i.e., Debye−Waller factors) for each of the individual chromate equilibrium species. The emphasis for this XAFS investigation is placed on the structural differences between the bi- and dichromate species, which has not been the focus of previous XAFS investigations.[14,15] Indeed, the results we obtain from this XAFS investigation on the structure of the bi- and dichromate species are important in explaining and supporting the conclusions we derive from the IR measurements: that the bichromate species indeed exists and must have Cr−O bond distances nearly identical to those found in the dichromate species.

The knowledge of the structure and speciation in the aqueous chromate system is useful for a number of applications.[6] The most recent motivations to study aqueous chromium solutions stem from environmental concerns. Chromium(VI) compounds are strongly carcinogenic. Aqueous chromates are highly mobile species in the groundwater; therefore, there is a strong need to remove Cr(VI) compounds from contaminated soils.

Chromium species are also present in much of the radioactive wastes at various Department of Energy (DOE) sites, and these are waiting to be vitrified into stable-glass waste forms. At the Hanford Site, for example, it is planned that radioactive wastes that are currently stored in underground storage tanks will be processed and separated into high-activity (primarily solids) and low-activity (primarily liquids) fractions and then vitrified. Although in both the high-activity waste (HAW) and the low-

* Corresponding author. Fax: (509) 376-0418. E-mail: jl_fulton@pnl.gov.
§ Present address: Department of Chemistry, State University of New York at Brockport, Brockport, NY 14420.
† Fundamental Sciences Division.
‡ Energy Science & Technology Division.

10.1021/jp0027041 CCC: $20.00
Published on Web 02/08/2001

activity waste (LAW) radionuclides are of obvious concern, it is often the nonradioactive components, such as chromium species, that are troublesome from a vitrification standpoint.[16]

For example, the solubility limit of Cr_2O_3 in some LAW glass formulations has been determined to be less than about 1 wt %.[16] In some cases, then, the amount of chromium in the waste could limit the waste loading into the glass, which affects the economics of the waste cleanup effort. In HAW glass melts, the interactions between Cr_2O_3, FeO, Fe_2O_3, NiO, and other oxides result in the formation of spinel crystals in the melt, which can cause problems during vitrification, and thus limit waste loading.[17] It is for these reasons that researchers are studying methods of hydrothermally oxidizing the relatively insoluble Cr(III) oxyhydroxides which occur in the waste sludges to soluble Cr(VI) species, thus creating the possibility of using aqueous chromium separation schemes to decrease the concentration of chromium in the wastes that enter the vitrification plant.

The high-temperature treatment of these waste streams, and the implementation of possible chromium separation schemes from the waste streams, both require an understanding of the chromium speciation and structure with respect to high temperatures. The results presented here for ambient conditions represent the first part of an IR and XAFS investigation of the aqueous chromate species. An extension of this study to higher temperatures is the subject of a second publication.[18]

Experimental Section

As previously described,[19] a short path length IR flow cell was used for the acquisition of the IR spectra, using a Bruker IFS66V FT-IR instrument. The IR experiments needed to be conducted in deuterated water in order to avoid overlapping H_2O bands in the spectral region of interest, although, generally speaking, bands that are above approximately 875 cm^{-1} may also be investigated using normal H_2O water. Solutions were prepared from solid $Na_2CrO_4 \cdot H_2O$ (99%) or $Na_2Cr_2O_7 \cdot H_2O$ (99%) that was dried overnight at 150 °C to remove the waters of crystallization. Deuterated 65 wt % nitric acid and 40 wt % sodium hydroxide solutions were used for adjusting the solution pH. Due to the short optical path length of 25 μm that was used, there were oscillatory interference fringes in the data that were removed by subtracting a pure D_2O spectrum. The IR vibrational bands were deconvoluted by fitting to Gaussian-shaped peaks using the Levenberg−Marquardt method.[20]

In this report, XAFS refers to the combined spectral regions of the X-ray absorption near-edge structure (XANES) and extended X-ray absorption fine structure (EXAFS). The XANES region is approximately 50 eV below to 50 eV above the absorption edge E_o, and the EXAFS is discernible in the region from 50 to 1000 eV above the edge. The XAFS data were acquired in fluorescence mode using an argon-filled ion chamber as the detector. The XAFS experiments were conducted on the PNC-CAT beam line (ID-20) at the Advanced Photon Source (APS) at Argonne National Laboratory. Both the undulator and the monochromator (Si 111 crystal) were scanned for XAFS spectra acquisition. To reject higher harmonics, the X-ray beam was reflected by a gold-plated mirror that was placed just upstream of the cell and the first ion chamber. As a further measure, the monochromator was detuned 30%. The energy stability of the monochromator was monitored with appropriate standards during all measurements.

A flow cell with Kapton windows and path length of 3.1 mm was constructed for the XAFS measurements. We found that it was necessary to continuously flow the aqueous chromate samples during XAFS data acquisition (approximately 25 min per scan) because it was observed that the chromate solutions reacted slowly with the Kapton window film to produce a solid Cr(III) compound. The continuous flow of fresh solution slowed the reaction rate. For each sample scan, evidence of Cr(III) contamination in the data could be determined by acquiring a pure water scan before and after each sample run. The Cr(III) impurities accounted for less than 2% of the spectral intensities for the 1.45 and 0.145 *m* samples and less than 5% for the 14.5 m*m* solutions.

Procedures for the EXAFS data reduction are well established[21,22] and involve the removal of a background function, and subsequent fitting of the thereby obtained EXAFS oscillations, $\chi(k)$. Standard algorithms were employed for these procedures.[23,24] The standard EXAFS equation

$$\chi(k) = \frac{F(k){S_0}^2 N}{kR^2} e^{-2k^2\sigma^2} e^{-2R/\lambda(k)} \sin\left(2kR + \delta(k) - \frac{4}{3}k^3 C_3\right) \quad (4)$$

was used to fit the aqueous chromate EXAFS data, where $F(k)$, $\delta(k)$, and $\lambda(k)$ are the amplitude, phase, and mean-free path factors, respectively, that were derived from the theoretical standard known as the FEFF code.[25] The Debye−Waller (DW) factor, σ^2, represents the mean-square variation of the shell distance *R*. The anharmonicity of the pair distribution, C_3, and a single nonstructural parameter, ΔE_o, were both kept constant during the final fitting of the data to the refined values of $C_3 = -5 \times 10^{-5}$ Å^{-3} and $\Delta E_o = -7$ eV.

The constant core-hole factor S_0^2 (0.95) was determined by fitting the high pH data, where the tetrahedral CrO_4^{2-} monomer unit is dominant and the Cr−O coordination number, *N*, is 4. All radial structure plots, $|\tilde{\chi}(R)|$, presented are derived from the magnitudes of the Fourier transformations of k^2-weighted $\chi(k)$ functions from $1.5 < k < 15$ Å^{-1} employing Hanning windows. A fractional misfit $\mathcal{R}$ according to

$$\mathcal{R} = \frac{\sum_{i=1}^{N} |\tilde{\chi}^{\mathrm{fit}}(R_i) - \tilde{\chi}^{\mathrm{exp}}(R_i)|^2}{\sum_{i=1}^{N} |\tilde{\chi}^{\mathrm{exp}}(R_i)|^2} \quad (5)$$

was calculated in order to evaluate the goodness of fit to the experimental data, where a smaller $\mathcal{R}$ value implies a better fit to the data.[24,26]

Results and Discussion

A. IR Spectra. The equilibrium constants for eqs 1−3 are

$$K_1 = \frac{a_{HCrO_4^-}}{a_{CrO_4^{2-}} a_{H^+}} = \frac{\gamma_{HCrO_4^-}}{\gamma_{CrO_4^{2-}} \gamma_{H^+}} \frac{m_{HCrO_4^-}}{m_{CrO_4^{2-}} m_{H^+}} = \frac{\gamma_{HCrO_4^-}}{\gamma_{CrO_4^{2-}} \gamma_{H^+}} K_{m,1} \quad (6)$$

$$K_2 = \frac{a_{Cr_2O_7^{2-}}}{a^2_{CrO_4^{2-}} a^2_{H^+}} = \frac{\gamma_{Cr_2O_7^{2-}}}{\gamma^2_{CrO_4^{2-}} \gamma^2_{H^+}} \frac{m_{Cr_2O_7^{2-}}}{m^2_{CrO_4^{2-}} m^2_{H^+}} = \frac{\gamma_{Cr_2O_7^{2-}}}{\gamma^2_{CrO_4^{2-}} \gamma^2_{H^+}} K_{m,2} \quad (7)$$

$$K_3 = \frac{a_{Cr_2O_7^{2-}}}{a^2_{HCrO_4^-}} = \frac{\gamma_{Cr_2O_7^{2-}}}{\gamma^2_{HCrO_4^-}} \frac{m_{CrO_7^{2-}}}{m^2_{HCrO_4^-}} = \frac{\gamma_{Cr_2O_7^{2-}}}{\gamma^2_{HCrO_4^-}} K_{m,3} \quad (8)$$

where *a* is the activity of the individual species that can be expressed in terms of the ionic activity coefficient γ and the actual species concentration *m* in molality units. Furthermore, the equilibrium constant K_3 can be expressed in terms of the

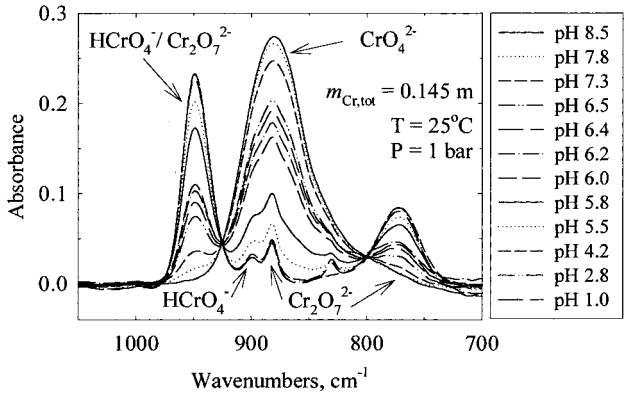

Figure 1. IR spectra of aqueous chromate solutions as a function of solution pH at ambient conditions. The intense CrO_4^{2-} band, present at high pH conditions, is gradually replaced by two strong and two weak bands at low pH values, giving rise to two isosbestic points near 925 and 800 cm^{-1}. The total chrome concentration was 0.145 *m*.

equilibrium constants K_1 and K_2

$$K_3 = \frac{K_2}{(K_1)^2} \tag{9}$$

Based on the large body of previous investigations measuring the equilibrium constants of eqs 6−8,[1−7] the chromate species is dominant at high solution pH and is replaced at low pH conditions by the bi- and dichromate ions as the dominant species. There are unresolved questions about the existence of the bichromate species and questions about its structure and vibrational modes.[9,10] Thus, we conducted two IR experiments to address these questions. First, we acidified an aqueous chromate solution to low pH values and observed how changing the pH affects the IR spectrum. This experiment is presented in Figure 1. Next, we measured the IR spectrum as a function of the total chrome concentration at a fixed pH value of about 3. At this pH value the reported equilibrium constants[1−7] predict that the bi- and dichromate systems are the only dominant species present. Thus, by changing the total chrome concentration the relative mole fractions of the bi- and dichromate species should change. If no bichromate existed and only the dichromate was present at low pH conditions, no spectral changes would be expected with variation of the total chrome concentration. This dilution experiment is presented in Figure 2. Finally, we present results from a quantitative analysis of the IR spectra, presented in Figures 1 and 2, that provides verification of spectral assignments and allows for the evaluation of the equilibrium constants from the IR band intensities that can then be compared with previously reported values. These results are summarized in Tables 1−3 .

There is one technical detail with regard to the quantitative analysis of the spectra in Figures 1 and 2 that deserves specific attention in order to avoid confusion. In Tables 2 and 3 we report the mole fractions $x_{Cr,mo}$, $x_{Cr,bi}$, and $x_{Cr,di}$. These are the mole fractions of chrome present as chromate (monomer), bichromate, and dichromate that are directly obtainable from the IR band intensities. While the number of chrome atoms must always be conserved, the number of chrome species is changing with the formation of dichromate, as it possesses two chrome atoms in its structure. Hence, the choice of "atom-based" mole fractions not only results in quantities that are more directly obtainable from the IR band intensities, but also avoids recalculation of all mole fractions relative to the total number of species present at each experimental condition. The species

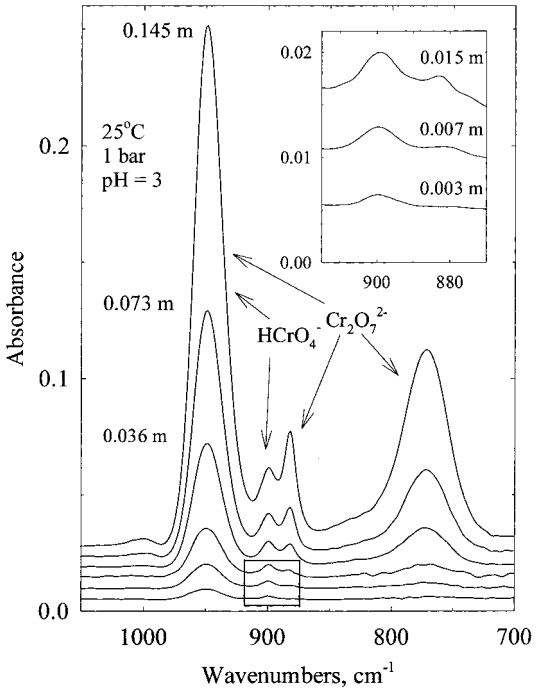

Figure 2. IR spectra of aqueous chromate solutions of pH 3 at ambient conditions as a function of total chrome concentration. The presence of two equilibrium species, i.e., the bi- and dichromate, is indicated by the change in the relative intensities of the two bands at 899 and 882 cm^{-1}.

TABLE 1: IR Band Characterization

frequency cm^{-1}	halfwidth[a] cm^{-1}	$\epsilon \times 10^5$ kg/(mol m)	species	mode
949 ± 1	25−30 ± 3	5.62 ± 0.11	$HCrO_4^-$	$\nu_{as}(CrO_3)$
949 ± 1	25−30 ± 3	11.29 ± 0.11	$Cr_2O_7^{2-}$	$\nu_{as}(CrO_3)$
899 ± 1	15 ± 2	1.48 ± 0. 03	$HCrO_4^-$	?
882 ± 1	13 ± 2	2.98 ± 0. 03	$Cr_2O_7^{2-}$	?
880 ± 1	63± 6	7.04 ± 0.14	CrO_4^{2-}	$\nu_{as}(CrO_4)$
773 ± 1	42 ± 4	5.70 ± 0. 05	$Cr_2O_7^{2-}$	$\nu_{as}(CrOCr)$

[a] Full width at half-maximum of band.

molalities m_{mo}, m_{bi}, and m_{di} are easily obtained from the reported total chrome concentration $m_{Cr,tot}$,

$$m_{mo} = m_{Cr,tot}\, x_{Cr,mo}, \quad m_{bi} = m_{Cr,tot}\, x_{Cr,bi}, \quad m_{di} = m_{Cr,tot}\,(1/2) x_{Cr,di} \tag{10}$$

and are included for convenience in Tables 2 and 3.

Similarly, the molal absorption coefficient, ϵ_i, for the species *i* is defined by the Beer−Lambert law

$$A_i = \epsilon_i m_i b \tag{11}$$

where A_i is the absorptivity at the frequency of the maximum of band *i*, m_i is the concentration in molality units of the corresponding species *i*, and *b* is the optical path length. In the usual convention, ϵ_i is expressed in reference to the species concentration and not in reference to the concentration of the absorbing sites. Although we adhere to this usual convention in the reported ϵ values of Table 1, it is also useful to compare the absorption coefficient of the $\nu_{as}(CrO_3)$ mode in the bi- and dichromate on a "per absorber" basis. Since there are two CrO_3 units present in the dichromate ion, the corresponding ϵ value in Table 1 needs to be divided by the factor of 2 for such a "per absorber" comparison.

TABLE 2: Dilution of an Aqueous Chrome Solution at a Low Solution pH of 3, Quantitative Results from IR Spectra

	band									
$m_{Cr,tot}$ mol/kg	949 $x_{Cr,bi} + x_{Cr,di}$[a]	899 $x_{Cr,bi}$	882 $x_{Cr,di}$[a]	773 $x_{Cr,di}$[a]	899 + 882 $x_{Cr,bi} + x_{Cr,di}$[a]	899 + 773 $x_{Cr,bi} + x_{Cr,di}$[a]	m_{bi} mol/kg	m_{di} mol/kg	$\log(K_{m,3})$	$\gamma_{Cr_2O_7^{2-}}/(\gamma_{HCrO_4^-})^2$
0.003	1.073	0.745	0.202	0.305	0.947	1.091	0.00224	0.00038	1.88	1.00
0.007	0.991	0.639	0.372	0.381	1.011	1.020	0.00448	0.00132	1.82	0.87
0.015	0.997	0.551	0.446	0.442	0.996	0.992	0.00826	0.00333	1.69	0.64
0.036	1.003	0.431	0.584	0.566	1.015	0.997	0.01552	0.01035	1.63	0.57
0.073	0.995	0.361	0.630	0.632	0.991	0.994	0.02638	0.02303	1.52	0.44
0.145	1.045	0.317	0.735	0.727	1.052	1.044	0.04602	0.05298	1.40	0.33
0.725	1.121	0.221	0.747	0.746	0.968	0.967	0.16036	0.27055	1.02	0.14
1.450	-	0.208	0.789	0.789	0.997	0.997	0.30183	0.57176	0.80	0.08

[a] x_{di} refers to the mole fraction of chromium present as dichromate (there are two chromium atoms present in the dichromate molecule).

TABLE 3: Acidification of a 0.145 m Chromate Solution, Quantitative Results from IR Spectra

	band											
pH	880 $x_{Cr,mo}$	949 $x_{Cr,bi} + x_{Cr,di}$[a]	773 $x_{Cr,di}$[a]	949−773 $x_{Cr,bi}$	880 + 949 $x_{Cr,mo} + x_{Cr,bi} + x_{Cr,di}$[a]	m_{mo} mol/kg	m_{bi} mol/kg	m_{di} mol/kg	$\log K_{m,1}$	$\log K_{m,2}$	$\log K_1$	$\log K_2$
6.5	0.699	0.296	0.253	0.043	0.995	0.101	0.006	0.018	5.87	13.55	6.23	13.78
6.4	0.649	0.378	0.305	0.074	1.028	0.094	0.011	0.022	5.85	13.50	6.21	13.73
6.2	0.572	0.425	0.323	0.102	0.997	0.083	0.015	0.023	5.72	13.23	6.07	13.47
6.0	0.525	0.474	0.346	0.129	0.999	0.076	0.019	0.025	5.56	12.94	5.92	13.17
5.8	0.257	0.789	0.530	0.260	1.046	0.037	0.038	0.038	5.72	13.34	6.08	13.58
5.5	0.126	0.944	0.622	0.322	1.071	0.018	0.047	0.045	5.76	13.43	6.11	13.66

[a] x_{di} refers to the mole fraction of chromium present as dichromate (there are two chromium atoms present in the dichromate molecule).

We begin now with the description of the spectral changes that are observed in Figures 1 and 2. In the IR spectrum for a 0.145 *m* chromate solution at pH 8.5, shown in Figure 1, there is only one strongly absorbing band in the spectral region of 700−1100 cm^{-1}, at 880 cm^{-1}, that is assigned to the chromate species. This band is also Raman active and has previously been assigned as the ν_3 asymmetric stretching mode.[9,27] Upon acidification with nitric acid (deuterated), the IR spectra in Figure 1 show that the monomer band is replaced by two strong bands at 949 and 773 cm^{-1} and two weak bands at 899 and 882 cm^{-1}. The intensities of these new bands increase until a pH of about 4.2 is reached. At lower pH values, the spectra remain essentially unchanged. The weak band at 830 cm^{-1} is assigned to a mode of NO_3^-, and it is attributed to the nitric acid that was added to lower the solution pH. This band is not present in the spectrum labeled "pH 4.2" that was prepared from an aqueous solution containing only dissolved sodium dichromate salt.

There are two isosbestic points, spectral points with constant absorbancy, that are discernible in Figure 1; these occur near 925 and 800 cm^{-1}. The presence of isosbestic points implies that the position and shape, i.e., the full width at half-maximum, of the spectral features in Figure 1 remain unchanged upon acidification. Only the intensities of the spectral features change. Furthermore, each of the two singular isosbestic points in Figure 1 indicates equilibrium between two absorbers.[28]

Figure 2 shows aqueous chromate IR spectra with varying total chrome concentration, $m_{Cr,tot}$, but with a fixed pH value of about 3. If indeed both the di- and bichromate species are present, then their concentrations and the relative intensities of the corresponding IR bands should change as a function of $m_{Cr,tot}$. It is immediately discernible from Figure 2 that the intensity of the 899 cm^{-1} band relative to the 882 cm^{-1} band dramatically changes as a function of $m_{Cr,tot}$. At low concentrations the 899 cm^{-1} band becomes dominant, while the 882 cm^{-1} band is dominant at high concentrations. This observation is direct evidence for the presence of two equilibrium species and supports the generally accepted speciation model, as presented in eqs 1−3. Since the reported equilibrium constants for these low pH conditions predict that the bichromate is dominant at low $m_{Cr,tot}$ and that the dichromate is favored at high $m_{Cr,tot}$, we assign the 899 cm^{-1} band to the bichromate species and the 882 cm^{-1} band to the dichromate species.

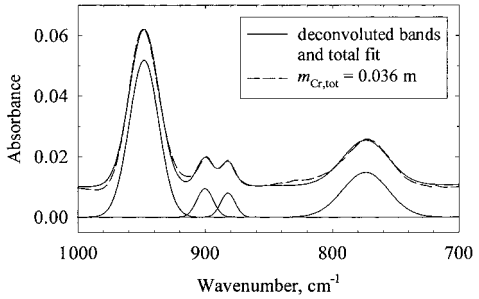

Figure 3. Example of a quantitative analysis of the IR spectra shown in Figure 2. Shown are the deconvoluted bands and total fit to the spectrum obtained from a 0.036 *m* aqueous chromate solution of pH 3.

To extract the equilibrium constant K_3 from the spectra in Figure 2 and to complete the band assignments, the spectra of Figure 2 were deconvoluted into four bands by fitting to Gaussian line shapes. This produced reasonable fits to the experimental spectra, as demonstrated for one example in Figure 3, that shows the spectrum and fit for an aqueous chromate solution of pH 3 with $m_{Cr,tot} = 0.036$ *m*. As reported in Table 1, only the half-width (full width at half-maximum) of the 949 cm^{-1} band increased systematically from 25 cm^{-1} at high total chrome concentration to 30 cm^{-1} at low total chrome concentration, while all other bands, as expected, had constant half-widths. The frequency of the 949 cm^{-1} band, as well as of all other bands, remained unchanged within ±1 cm^{-1} even while varying the total chrome concentration. The frequency and half-width of each band are summarized in Table 1.

By definition, the mole fractions *x* of all absorbing sites in the present chrome species add up to 1, and at conditions of pH 3, only the bi- and dichromate species are predicted to be present within the speciation model of eqs 1−3 and 6−8. Indeed,

we also observe no chromate at this pH, as evidenced by the lack of any broad peak at 880 cm^{-1}. So we obtain

$$1 = x_{Cr,bi} + x_{Cr,di} = m_{Cr,bi}/m_{Cr,tot} + m_{Cr,di}/m_{Cr,tot} \quad (12)$$

where m is the molal concentration, and the subscripts "Cr,bi" and "Cr,di" refer to chrome atoms present as bi- and dichromate, respectively, as previously explained. Using the Beer−Lambert law of eq 11 we obtain

$$1 = A_{899}/(m_{Cr,tot}\epsilon_{899}b) + A_{882}/(m_{Cr,tot}\epsilon_{882}b) \quad (13)$$

where the number subscripts specify the band. Since the optical path length is known (2.54 μm), ϵ_{899} and ϵ_{882} can be obtained by least-squares fitting the series of measured quantities $A_{899}/m_{Cr,tot}$ and $A_{882}/m_{Cr,tot}$ to eq 13. Hence, the mole fractions $x_{Cr,bi}$ and $x_{Cr,di}$ can be determined for each experimental condition, as reported in Table 2. It is interesting to observe that the molal absorption coefficients for the 899 and 882 cm^{-1} bands listed in Table 1 are, within experimental uncertainty, the same when compared on a "per absorber" basis, i.e., dividing ϵ_{882} by a factor of 2 to account for the two infrared absorbers per dichromate molecule. We do not have an exact assignment for the 899 and 882 cm^{-1} bands, although it is conceivable that these bands may be combination bands that include bending modes.

Analysis of the band at 773 cm^{-1} showed that its intensity scales with the intensity of the 882 cm^{-1} band; this indicates that it should be assigned to the dichromate species. This finding is in accordance with the band assignment made for solid dichromate, where this band is attributed to the $\nu_{as}(CrOCr)$ asymmetric stretching mode of the Cr−O bonds of the Cr−O−Cr bridge.[27] Hence, the 773 cm^{-1} band provides a second measure for the mole fractions $x_{Cr,di}$ by analyzing it with the 899 cm^{-1} band, using the same method described above. Indeed, the mole fractions $x_{Cr,di}$ obtained from the 773 cm^{-1} band agree very well with the mole fractions $x_{Cr,di}$ obtained from the analysis of the 882 cm^{-1} band, except for at the lowest concentration (0.003 m).

The $K_{m,3}$ values can be directly obtained from the mole fractions $x_{Cr,bi}$ and $x_{Cr,di}$, and they are included in Table 2 as $\log K_{m,3}$. On the other hand, knowledge of the ionic activity coefficients is required in order to evaluate K_3 so that it can be compared to values reported in the literature. Experimentally, only mean activity coefficients of an electrolyte X_aY_b can be obtained according to

$$\gamma_{\pm} = (\gamma_+^a + \gamma_-^b)^{1/(a+b)} \quad (14)$$

For dilute concentrations, mean activity coefficients can be evaluated using the Debye−Hückel theory for dilute aqueous solutions at ambient conditions

$$\log \gamma_{\pm} = -0.509\, I^{1/2}\, |z_+ z_-|_i \quad (15)$$

where I is the ionic strength of the solution resulting from all present ions, and z is the charge of the ion. According to eq 8, we are considering a mixture of two dissolved salts, $NaHCrO_4$ and $Na_2Cr_2O_7$, of salt types XY and X_2Y. According to eq 15, within the dilute limit, $\log \gamma_{\pm}$ for $Na_2Cr_2O_7$ is twice as large as $\log \gamma_{\pm}$ for $NaHCrO_4$. Hence, we know that

$$\log\left(\frac{\gamma_{Na_2Cr_2O_7}}{\gamma^2_{NaHCrO_4}}\right) = 2 \log \gamma_{NaHCrO_4} - 2 \log \gamma_{NaHCrO_4} = 0 \quad (16)$$

and we may set $K_3 = K_{3,m}$ at the lowest concentration of $m_{Cr,tot}$ = 0.003 m within the dilute limit range of the Debye−Hückel theory. The thereby obtained experimental $\log K_3$ value of 1.88 is in good agreement with published equilibrium constants that range from 1.6 to 2.16.[1−7] This furnishes further confidence in the validity of the commonly accepted speciation model for the chromate system and affirms the band assignments that have been made thus far. We then used the $\log K_3$ value of 1.88 that was obtained to calculate $\gamma_{Cr_2O_7^{2-}}/\gamma^2_{HCrO_4^-}$ for the higher concentrated solutions, as shown in Table 3.

We have not yet discussed the assignment for the 949 cm^{-1} band. Based on previous vibrational assignments for the solid dichromate[27] the 949 cm^{-1} band would be assigned to the $\nu_{as}(CrO_3)$ stretching mode; this mode should be present in both the bi- and dichromate molecule. However, we do not observe any splitting of this IR band for the two different species. This observation is similar to that made for the $\nu_s(CrO_3)$ symmetric stretching mode in the Raman.[9,10] The quantitative analysis of this band reveals that the 949 cm^{-1} band must be from two overlapping bands, one representing the bichromate and one representing the dichromate species. This conclusion is derived from the observation that A_{949} is directly proportional to the total chrome concentration, i.e., that $A_{949}/m_{Cr,tot}$ = constant over the entire range of investigated concentrations. Previously, we have shown that the bands at 899 and 882 cm^{-1} can be used to quantitatively determine the bichromate and dichromate concentrations. Hence, we can use a relationship similar to eq 13 to show that the 949 cm^{-1} band is a linear combination of the product of the dichromate and bichromate molal concentrations with their respective molal absorption coefficients, $\epsilon_{949,bi}$ and $\epsilon_{949,di}$. From the concentration series in Table 2, we fitted the individual ϵ_{949} values for the bichromate and dichromate that are reported in Table 1. As mentioned earlier, there are two $-CrO_3$ units present in the dichromate molecule, and thus, ϵ_{949} for the dichromate species is nearly twice the value found for bichromate.

The values in the second column of Table 2 were obtained by dividing $A_{949}/m_{Cr,tot}$ by $(\epsilon_{949,bi}x_{bi} + \epsilon_{949,di}x_{di})b$ which should result in values of 1. Deviations from 1 represent the combined errors of sample preparation and introduction into the IR cell, and quantitative peak analysis. There is no entry for the 1.45 m total chrome solution because the intensity of the 949 cm^{-1} band exceeded the dynamic range of the detector for this concentration.

Considering that the resonance frequency and the molar absorption coefficient of the $\nu_{as}(CrO_3)$ asymmetric stretching mode are nearly identical for both molecules, the structural parameters for the $-CrO_3$ unit, such as the bond length, must be extremely similar in the bi- and dichromate molecules. As we discuss later, the XAFS data confirm this conclusion. Furthermore, since we find that the resonance frequency of the $\nu_{as}(CrO_3)$ asymmetric stretching mode must be nearly identical for both the bi- and dichromate species, the frequency of the Raman active $\nu_s(CrO_3)$ symmetric stretching mode should be identical in both molecules as well. In addition, inspection of the peak heights of the Raman spectra for low-pH aqueous chrome solutions at three different concentrations, that are reported by Michel and Cahay,[9] seem to indicate that the Raman intensities of the bichromate and dichromate bands are similar.

We now turn to the analysis of the chromate, bichromate, and dichromate equilibria in Figure 1, and the evaluation of the equilibrium constants $K_{1,m}$ and $K_{2,m}$. For this analysis, the data in Table 1 gives the molal absorption coefficient of the strong 880 cm^{-1} monomer band that is needed. This absorption coefficient was obtained directly from the IR spectrum of the

aqueous chromate solution at pH 8.5 where only the chromate species exists.

In Figure 1, the mole fractions $x_{Cr,bi}$ and $x_{Cr,di}$ may in principle be obtained directly from the 899 and 882 cm^{-1} bands. However, in practice, deconvolution of these bands from the strong 880 cm^{-1} band resulted in a slight overestimation of the intensities of these weak bands. A more accurate result was obtained by using the more isolated and stronger 773 cm^{-1} band to determine $x_{Cr,di}$. Then $x_{Cr,bi}$ was obtained by subtracting the $x_{Cr,di}$ values from the total bichromate and dichromate mole fraction that was determined from the 949 cm^{-1} band. Using eqs 6 and 7, the log $K_{m,1}$ and log $K_{m,2}$ values, reported in Table 3, are obtained from the species mole fractions listed in Table 3, the known 0.145 *m* total chrome concentration, and the measured pH values. These values are only slightly below the values reported in the literature for log K_1 (6.03−6.55) and for log K_2 (13.99−14.70).[1−7] However, for direct comparison, knowledge of the mean ionic activity coefficients are needed in order to obtain the log K_1 and log K_2 values from the experimental log $K_{m,1}$ and log $K_{m,2}$ values that are reported in Table 3. A simple estimate of the ratio of activity coefficients in eqs 6 and 7 can be made. First, we assume that the activity coefficients of the monovalent bichromate and hydronium ions are equal. From the tabulated mean activity coefficients for various salts, we know that this assumption leads to errors of less than about 40 % at these high salt concentrations. Second, we derive the activity coefficient of 0.44 for the CrO_4^{2-} by interpolating published activity coefficients of the sodium chromate system.[29] From Table 2, we know that the value of $\gamma_{Cr_2O_7^{2-}}/\gamma^2_{HCrO_4^-}$ is 0.33. Thus we obtain,

$$\frac{\gamma_{HCrO_4^-}}{\gamma_{CrO_4^{2-}}\gamma_{H^+}} = \frac{1}{\gamma_{CrO_4^{2-}}} = \frac{1}{0.44} \tag{17}$$

$$\frac{\gamma_{Cr_2O_7^{2-}}}{\gamma^2_{CrO_4^{2-}}\gamma^2_{H^+}} = \frac{\gamma_{Cr_2O_7^{2-}}}{\gamma^2_{CrO_4^{2-}}\gamma^2_{HCrO_4^-}} = \frac{0.33}{(0.44)^2} \tag{18}$$

that are used to produce the log K_1 and log K_2 values listed in Table 3. The log K_1 values agree well with the values reported in the literature, the latter of which range from 6.03 to 6.55. Although they are somewhat low, our log K_2 values also compare reasonably well with the literature values that range from 13.99 to 14.7.[2,5,6] As a whole, the IR data from Figures 1 and 2 confirm the well-accepted model for the aqueous chromate system, with the bichromate, dichromate, and chromate as the major equilibrium species.

For very low pH conditions and high concentrations, the free chromic acid H_2CrO_4 and/or the free dichromic acid according to

$$CrO_4^{2-} + 2H^+ \rightleftharpoons H_2CrO_4 \tag{19}$$

$$Cr_2O_7^{2-} + 2H^+ \rightleftharpoons H_2Cr_2O_7 \tag{20}$$

may also be present as equilibrium species. According to equilibrium constants for eq 20 that have been reported to be log K_{eq20} = 5.14 and 5.06, [5,30] the concentration of the free acid in a 0.145 aqueous chromate solution of pH 3 should be 2−3 orders of magnitude smaller than the concentrations of the bi- or dichromate species. Indeed, the equilibrium constant K_3 we obtained from the quantitative spectral analysis does not deviate significantly from previous reported values even though we did not include the free chromic acid or the free dichromic acid in the analysis. The $\nu_{as}(CrO_2)$ asymmetric stretching band of the free acids should be in a similar frequency range as was observed for the chromyl halogenides, such as CrO_2Cl_2, where this strong band was found in the vicinity of 1000 cm^{-1}.[31,32] There is an indication in the spectra shown in Figure 2 of a weak band near 1000 cm^{-1} for concentrations exceeding 0.036 *m*. However, although this band should also be Raman active it is not observed in the reported spectrum for a 0.1 *m* chromate solution of pH 1.2.[9] Hence, at this point it is not conclusive if the weak 1000 cm^{-1} band can be assigned to the $\nu_{as}(CrO_2)$ asymmetric stretching band of the acids.

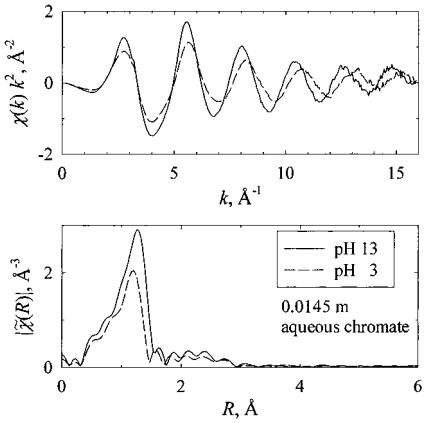

Figure 4. Two $\chi(k)$ functions (upper portion) with their corresponding radial structure plots, $\tilde{\chi}(R)$, (lower portion) for a 0.0145 *m* aqueous chromate solution at pH 13 and 3. The clearly discernible differences arise from the different first shell environment around the central chrome atom in the CrO_4^{2-} and the $HCrO_4^-/Cr_2O_7^{2-}$ structures, as explained in the text.

B. EXAFS Spectra. In this section, we explore the structural differences between the bichromate and dichromate molecules. According to the IR results summarized in Table 2, the ratio of bi- to dichromate changes from approximately 1:4 at 1.45 *m* total chrome concentration to 1:1 at 0.015 *m* total chrome concentration. If there are significant structural differences between the bi- and dichromate molecule, with regard to the chrome−oxygen bond distances, changing the total chrome concentration should measurably affect the EXAFS results. Therefore, we acquired EXAFS spectra of three aqueous chromate solutions of pH 3 with varying total chrome concentration (1.45, 0.145, and 0.0145 *m*) to investigate this matter. This range of concentration is easily detectable by EXAFS. We also acquired EXAFS spectra for aqueous chromate at pH 13 for the same three concentrations, which served as a reference. At these high pH conditions, only the chromate CrO_4^{2-} is present, regardless of the total chrome concentration, and no changes are expected to be present in these EXAFS spectra with varying total chrome concentration.

To understand how structural changes in the chromate systems affect the EXAFS it is instructive to first compare the EXAFS of CrO_4^{2-}, present at high-pH conditions, with the EXAFS of a $HCrO_4^-/Cr_2O_7^{2-}$ mixture, present at low-pH conditions. The corresponding two $\chi(k)$ functions presented in the upper portion of Figure 4 differ significantly. The $\chi(k)$ oscillations of the pH 3 solution are lower in amplitude and are shifted to higher *k* values than the $\chi(k)$ oscillations for the pH 13 solution. These observations can be qualitatively explained by the structural differences between the CrO_4^{2-} and $Cr_2O_7^{2-}$ anions that are well documented from studies of solid chromate and dichromate compounds.[33−35] As qualitatively depicted in Figure 5, the chromate monomer ion is of perfect tetrahedral symmetry, having only one chrome−oxygen (Cr−O) bond distance. In

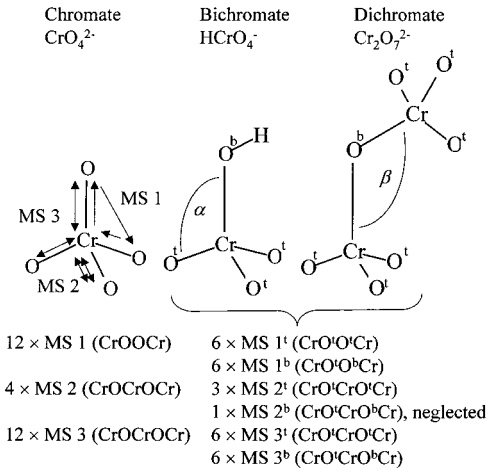

Figure 5. Schematic representation of the CrO_4^{2-}, $HCrO_4^-$and $Cr_2O_7^{2-}$ structures and their principle multiple scattering (MS) paths.

contrast, the local first-shell environment of the chrome atoms in the dichromate ion is of C_{3v} symmetry, involving three equivalent bonds to terminal oxygen (O^t) atoms and one bond to the bridging oxygen atom (O^b). For the $HCrO_4^-$ anion, the local chrome symmetry is also expected to be C_{3v}. However, the Cr−O^t and Cr−O^b bond distances may differ from those of the $Cr_2O_7^{2-}$ anion. Bearing these structural differences in mind, the lower amplitude of the $\chi(k)$ function for the low-pH solution, in the upper portion of Figure 4, arises from the destructively interfering single scattering contributions from the nonuniform chrome−oxygen bond distances present in the bi- and dichromate molecules. A similar effect has been observed in the isopolytungstate system.[36] The observed phase shift to higher k values in the $\chi(k)$ function for the low pH solution indicates the presence of chrome−oxygen bond distances (the Cr−O^t bonds) that are shorter than the Cr−O bond distance in the CrO_4^{2-} ion.

The corresponding radial structure plots, i.e., the magnitude of the Fourier Transforms of the $\chi(k)$ functions from the k-range of 1.5−15 Å^{-1}, are presented in the lower portion of Figure 4. The lower amplitude of the $\chi(k)$ function for the low pH solution results in a less intense main peak for the Cr−O single scattering contributions in the radial structure plot. It is interesting to observe that the maximum of the main peak is shifted to a slightly lower R-value for the low pH solution. This indicates that there are Cr−O bond distances in the bi-/dichromate structures (the Cr−O^t bonds) that are shorter than the Cr−O bond distance in the CrO_4^{2-} ion. This is in keeping with the observation made for the IR spectra of Figure 1, that the $\nu_{as}(CrO_3)$ mode is shifted 69 cm^{-1} to a higher frequency than the corresponding $\nu_{as}(CrO_4)$ mode of the CrO_4^{2-} ion. The shorter Cr−O^t bond distance was previously explained by an increase of the Cr−O bond order, that is, the Cr−O^t bonds are of more double bond in character than the Cr−O bonds in the CrO_4^{2-} ion.[32] The 3:1 weighting of the three short Cr−O^t bonds to the one long Cr−O^b bond causes the maximum of the main peak to appear at a lower R value in the radial structure plot.

In the radial structure plots of Figure 4 there are also significant contributions from multiple scattering (MS) paths that are discernible in the range from 1.8 to 3 Å. For the dichromate ion, Cr−Cr single scattering contributions are also to be expected in this R range. MS path contributions also become apparent in the $\chi(k)$ functions as deformations of the sinusoidal wave pattern at low k values. The significance of MS contributions for the CrO_4^{2-} system has been previously discussed in detail.[15] The principal MS paths are depicted in Figure 5 for the CrO_4^{2-} structure and involve a 12-fold degenerate triangular path MS 1 (CrOOCr), a 4-fold degenerate path MS 2 (CrOCrOCr), and a 12-fold degenerate path MS 3 (CrOCrOCr). The MS 2 path represents a double backscattering from the same oxygen atom, while the MS 3 path involves backscattering from two different oxygen atoms. The nonequivalence of the four oxygen atoms in the bi- and dichromate structure splits the degeneracy of these MS paths, as indicated in Figure 5.

Figure 6 presents the $\chi(k)$ functions with the corresponding radial structure plots for the low-pH, aqueous chromate solutions with varying total chrome concentration. Compared to the clear differences of the $\chi(k)$ functions for the chromate and the bi-/dichromate mixture in Figure 4, differences are hardly discernible in either the $\chi(k)$ functions or the corresponding radial structure plots of Figure 6. This is despite the fact that the ratio of bi- to dichromate changes from approximately 1:4 at 1.45 m total chrome concentration to 1:1 at 0.0145 m total chrome concentration. From this qualitative observation alone, we may conclude that the local first-shell environment around the chrome atom must be structurally very similar between the bi- and dichromate ion. Even upon close inspection of the radial structure plots in Figure 6, only minor trends are directly observable. A very small decrease of the main peak intensity with decreasing total chrome concentration is noted. This may indicate a slightly increased incoherence of Cr−O bond distances in the 1:1 mixture of bi- and dichromate species at 0.0145 m total chrome concentration. Also, a slight decrease of the intensities of the peaks near 2.4 and 2.8 Å with decreasing total chrome concentration may reflect the declining Cr−Cr single scattering contributions at lower total chrome concentrations.

The Debye−Waller (DW) factors of MS paths are typically much larger than the DW factors of single scattering paths. Hence, MS paths contribute mainly to the $\chi(k)$ function at low k values, as defined by eq 4. As a consequence, we observed that the multiple scattering contributions were largely suppressed in the radial structure plots when the Fourier Transform was performed for the k range of 6−15 Å^{-1}. With this in mind, we carried out the EXAFS analysis in two ways. First, we analyzed the EXAFS data using only a k range from 6−15 Å^{-1} and an R range of 1−2 Å (EXAFS analysis I). This allowed us to exclude the rather complicated MS contributions (and the Cr−Cr single scattering contribution) and to focus the analysis only on the Cr−O single scattering path contributions. In the second refined analysis (EXAFS analysis II), a k range of 1.5−15 Å^{-1} and an R range of 1.0−3.5 Å was used in order to fit the multiple scattering and Cr−Cr single scattering contributions to the data.

i. EXAFS Analysis I. As explained in the Experimental Section, the high-pH CrO_4^{2-} EXAFS data served to determine the fitting parameters S_0^2, ΔE_0, and C_3; since the oxygen coordination number is known for this system only two structural fit parameters are left to be determined, namely the Cr−O bond distance and the corresponding DW factor. Once the best values for S_0^2, ΔE_0, and C_3 were obtained, these were held constant throughout all remaining EXAFS data analyses. As mentioned earlier, the high-pH CrO_4^{2-} EXAFS data also serve as another type of reference set. Since the CrO_4^{2-} species remains the only significant equilibrium species at these high pH conditions regardless of the total chrome concentration, the EXAFS spectra should remain unchanged. This is an important aspect because we expected to observe self-absorption effects in the data at high Cr concentrations that may cause amplitude distortions in the EXAFS oscillations. These distortions arise

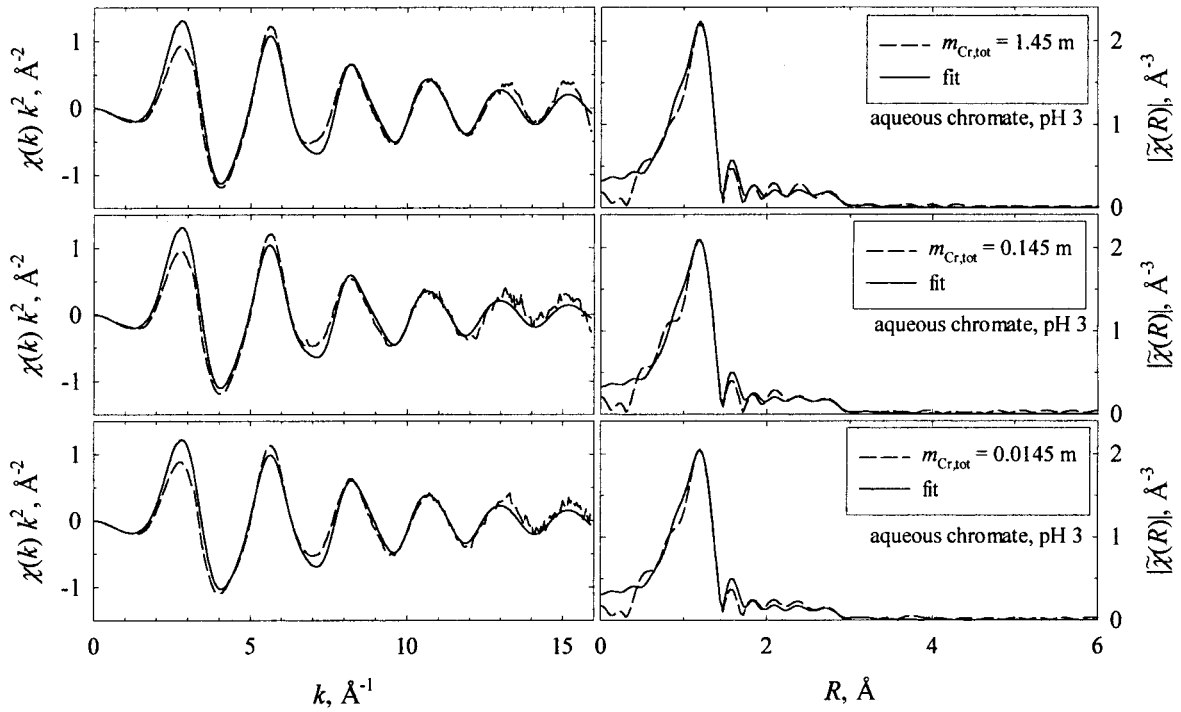

Figure 6. The $\chi(k)$ functions (left) with their corresponding radial structure plots, $\tilde{\chi}(R)$, (right) for three aqueous chromate solutions at pH 3 having a total chrome concentration of 1.45 (top), 0.145 (middle), and 0.0145 *m* (bottom). Although the ratio of bi- to dichromate changes from 1:4 at 1.45 *m* to 1:1 at 0.0145 *m*, the spectral differences are hardly discernible, suggesting a high degree of structural similarity between the bi- and dichromate molecular ions.

TABLE 4: EXAFS Analysis I (Fit Range: 6 Å^{-1} < k < 15 Å^{-1} and 1 Å < R < 2 Å)

$m_{Cr,tot}$ mol/kg	1.45	0.145	0.0145
	pH 13 Data		
R (Cr−O) (Å)	1.660 ± 0.003	1.660 ± 0.002	1.660 ± 0.001
σ^2 (Cr−O) × 10^{-3} Å^2	1.49 ± 0.27	1.68 ± 0.15	1.68 ± 0.11
R^a	0.014	0.005	0.003
	pH 3 Data		
R (Cr−O^t) (Å)	1.624 ± 0.002	1.623 ± 0.003	1.622 ± 0.003
R (Cr−O^b) (Å)	1.801 ± 0.010	1.796 ± 0.015	1.800 ± 0.021
σ^2 (Cr−O^t) × 10^{-3} Å^2	1.43 ± 0.16	2.13 ± 0.26	1.99 ± 0.24
σ^2 (Cr−O^b) × 10^{-3} Å^2	2.94 ± 0.857	3.62 ± 1.29	5.69 ± 1.97
R^a	0.002	0.005	0.004

[a] Fractional misfit as defined in eq 5.[24,26]

from the fact that for strongly absorbing samples the transmission increases at higher energies. For samples that absorb much more than one absorption length, this effect may lead to an overall reduction in amplitudes and to apparent larger EXAFS oscillations at high k values, resulting in apparently smaller DW factors.

The fit results for the high-pH solution, summarized in Table 4, show literally identical values for the Cr−O bond distance and corresponding DW factor for the 0.145 and 0.0145 *m* solutions. Hence, we are confident that self-absorption effects are not present in the 0.145 *m* data. In the 1.45 *m* data self-absorption effects were clearly evident, leading to a lower overall amplitude of the $\chi(k)$ function for these data.[37] However, by dividing by an amplitude correction factor, $A_0 = 0.70$, the $\chi(k)$ function is visually indistinguishable from the high pH $\chi(k)$ functions at lower concentrations. The same amplitude correction was applied to the low-pH, 1.45 *m* $\chi(k)$ function, as shown in the upper portion of Figure 6. Self-absorption does not affect the bond distance, as shown in Table 4, for the high-pH, 1.45 *m* solution where the same Cr−O bond distance[37] is obtained as in the less concentrated samples. Self absorption does affect the DW factor,[37] which is slightly smaller, but the deviation from the DW factors of the less concentrated samples is still within the uncertainty of the fit. We believe that the self absorption effects present in the 1.45 *m* data lead only to slight underestimates of the reported DW factors.

In the EXAFS analysis I, for the low pH data only, two types of Cr−O bonds are assumed to be present, one representing the average Cr−O^t bond distance, and the other representing the Cr−O^b bond distance present in the bi-/dichromate mixture, as indicated in Figure 5. If the Cr−O^t and Cr−O^b were significantly different in the bi- and dichromate structures, lowering the total chrome concentration from 1.45 to 0.015 *m* should reveal a change in the observed average bond distances and/or should increase the observed average DW factors. This is because the bi-/dichromate ratio changes from 1:4 to 1:1 upon dilution from 1.45 to 0.0145 *m*, and contributions to the DW factor from static disorder should increase. The fit results summarized in Table 4 do not support any significant trend with variation of the total chrome concentration, except for a systematic increase of the Cr−O^b DW factor at low total chrome concentrations. A very small decrease of the Cr−O^t bond distance by 0.002 Å is indicated, but the magnitude of this change is smaller than the uncertainty of the measurement. The results from the EXAFS analysis I support the conclusion that the local first-shell structure around the central chrome atom is very similar in the bi- and dichromate structures. The finding of an essentially identical Cr−O^t bond distance is supported by the observed overlap of the $\nu(CrO_3)$ symmetric and asymmetric vibrational modes. However, the finding that the Cr−O^b distance is the same in these two molecular ions is surprising when the greatly different chemical nature of the adjoining H atom or CrO_3 structural unit is considered. Indeed, the EXAFS analysis II sheds a different light on this issue, as explained below. Overall, the chrome−oxygen bond distances obtained from EXAFS analysis I compare favorably to the average Cr−O bond distances found in solid chromate and dichromate compounds, (1.645, 1.629, and 1.790 Å for the Cr−O, Cr−O^t, and

$Cr-O^b$ bonds, respectively)[35] and to previous reports on the aqueous chromate ion (1.67 Å[15] and 1.63 Å[14]).

ii. EXAFS Analysis II. For this more complete analysis, the multiple scattering (MS) paths shown in Figure 5 were included in the EXAFS analysis over a k range of 1.5−15 $Å^{-1}$ and an R range of 1−3.5 Å. For the low-pH data, the Cr−Cr single scattering path was also included by weighting the contributions to this path by the dichromate mole fractions, $x_{Cr,di}$, that were obtained from the IR measurements as summarized in Table 2. For the CrO_4^{2-} ion, the MS distances are given by

$$R_{(MS\ 1)} = R_{(Cr-O)} + R_{(Cr-O)} \sin(54.74) \quad (21)$$

$$R_{(MS\ 2)} = R_{(MS\ 3)} = 2R_{(Cr-O)} \quad (22)$$

where the argument of the sin function in eq 21 is half the tetrahedral angle. For the bi- and dichromate case, the MS path distances are given by

$$R_{(MS\ 1^t)} = R_{(Cr-O^t)} + R_{(Cr-O^t)} \sin(60) \sin(180\text{-}\alpha) \quad (23)$$

$$R_{(MS\ 1^b)} = (R_{(Cr-O^t)} + R_{(Cr-O^b)} + ((R_{(Cr-O^t)})^2 + (R_{(Cr-O^b)})^2 - 2R_{(Cr-O^t)} R_{(Cr-O^b)} \cos(\alpha))^{1/2})/2 \quad (24)$$

$$R_{(MS\ 2^t)} = R_{(MS\ 3^t)} = 2R_{(Cr-O^t)} \quad (25)$$

$$R_{(MS\ 2^b)} = R_{(MS\ 3^b)} = R_{(Cr-O^t)} + R_{(Cr-O^b)} \quad (26)$$

which introduces the O^tCrO^b bond angle α as a new variable that was initially included as a fitting parameter. A value of α = 106° ± 8° was obtained that did not vary significantly from the high- to low-concentration data and was therefore kept fixed for the final fit to the low-pH data. A similar value of α = 107.5° ± 4° was also found for the solid sodium dichromate.[35]

The geometrical constraints of eqs 21−26 that arise from inclusion of the MS paths should lead to a refined fit value for chrome−oxygen bond distances. In principle, each MS path may have a different DW factor associated with it. However, separate DW factors for the MS paths, MS 2 and MS 3, were too highly correlated and were, as a reasonable structural approximation, set equal to one another. Likewise, only two MS DW factors were used for the low-pH data, one DW factor for both the MS 1^t and MS 1^b paths and one DW factor for the MS 2^t, MS 3^t, and MS 3^b paths. The MS 2^b path was neglected because of the low degeneracy of this path.

The fit results from EXAFS analysis II that are listed in Table 5 compare favorably overall with the EXAFS analysis I results presented in Table 4. Particularly well confirmed is the $Cr-O^t$ bond distance that again is unchanging with total chrome concentration, i.e., under largely varying dichromate-to-bichromate ratios. The obtained Cr−Cr distance of 3.21 Å is of a similar value to the previously reported value of 3.18 Å,[14] and the Cr−Cr distance of 3.166 Å found in solid sodium dichromate.[35] The largest difference between the results of the two analysis schemes concerns the $Cr-O^b$ bond distance for the low-pH data, in the EXAFS analysis II, it is about 0.03 Å larger for the 1.45 and 0.145 m*m* solutions and increases to 1.876 Å for the 0.0145 *m* solution. In the EXAFS analysis I, this bond distance did not change with total chrome concentration. On the other hand, a systematic increase of the corresponding DW factor was observed in the EXAFS analysis I. Thus, both analyses indicate that there may be small changes in the $Cr-O^b$ bond character. It is difficult to judge from the more refined EXAFS analysis II results if the $Cr-O^b$ bond distance is indeed larger in the $HCrO_4^-$ structure, although this conclusion seems very plausible. The $Cr-O^b$ distance in the dichromate solid was found to be 1.791 Å, which is closer to the $Cr-O^b$ value that was obtained in the EXAFS analysis I. The $Cr-O^b-Cr$ bond angle β can be obtained from the knowledge of the Cr−Cr bond distance (3.21 Å) and the $Cr-O^b$ bond distance. Using the $Cr-O^b$ bond distance result for the 1.45 *m* solution at pH 3, where the dichromate is the dominant species, we obtain $\beta = 123°$ from the results of EXAFS analysis II. This value compares well with the reported $Cr-O^b-Cr$ bond angle of $\beta = 124°$ for solid dichromate.[35]

TABLE 5: EXAFS Analysis II (Fit Range: 1.5 $Å^{-1} < k <$ 15 $Å^{-1}$ and 1 Å $< R <$ 3.5 Å)

$m_{Cr,tot}$ mol/kg	1.45	0.145	0.0145
	pH 13 Data		
R (Cr−O) (Å)	1.656 ± 0.003	1.656 ± 0.003	1.656 ± 0.003
σ^2 (Cr−O) × 10^{-3} $Å^2$	1.68 ± 0.35	1.96 ± 0.34	1.84 ± 0.30
σ^2 (MS 1) × 10^{-3} $Å^2$	3.80 ± 7.06	2.60 ± 5.86	1.21 ± 4.59
σ^2 (MS 2), σ^2 (MS 3) × 10^{-3} $Å^2$	36.30 ± 33.44	37.15 ± 31.53	42.07 ± 33.28
R^a	0.038	0.035	0.026
	pH 3 Data		
R ($Cr-O^t$) (Å)	1.624 ± 0.003	1.624 ± 0.003	1.625 ± 0.002
R ($Cr-O^b$) (Å)	1.834 ± 0.022	1.824 ± 0.020	1.871 ± 0.018
R (Cr−Cr) (Å)	3.207 ± 0.026	3.213 ± 0.025	3.213 ± 0.026
σ^2 ($Cr-O^t$) × 10^{-3} $Å^2$	1.87 ± 0.29	2.61 ± 0.32	2.40 ± 0.25
σ^2 ($Cr-O^b$) × 10^{-3} $Å^2$	9.81 ± 3.52	10.64 ± 3.63	10.57 ± 2.98
σ^2 (Cr−Cr) × 10^{-3} $Å^2$	6.65 ± 3.04	6.38 ± 2.92	5.06 ± 2.89
σ^2 (MS 1) × 10^{-3} $Å^2$	6.52 ± 7.42	5.78 ± 6.04	6.00 ± 6.40
σ^2 (MS 2), σ^2 (MS 3) × 10^{-3} $Å^2$	29.13 ± 19.18	33.00 ± 19.80	22.21 ± 10.68
R^a	0.016	0.014	0.014

[a] Fractional misfit as defined in eq 5.[24,26]

The obtained DW factors for the MS paths overall have relatively large uncertainties. This is, in particular, true for the DW factor of the MS 2/MS 3 paths whose magnitude is also larger than expected. Since the photo electron travels essentially twice the distance of a chrome−oxygen single scattering path in these MS paths, one would expect the DW factor to be approximately the sum of the DW factors of the single scattering paths. One would also expect the DW factor of the MS 1 path to be larger than that of MS 2 and MS 3, since bending vibrations affect the effective path length of this MS path, but not of the MS 2 and 3 paths. However, considerably poorer-fit results were obtained when these constraints were forced onto the fitting model. Interestingly, Pandya also reports DW factors that are similar to those listed in Table 5.[15] The possibility of tightly bonded hydration water molecules has to be discounted as a possible explanation of this discrepancy, at least for the CrO_4^{2-} system, because of the long distance of the water hydration shell around chromate that has been measured by neutron and X-ray diffraction techniques.[38] In these studies, 12 water molecules were found to be at a shell distance of 3.96 Å; this is a distance that would approximately fall near 3.5 Å in the radial structure plot of Figure 6, where there are no significant features apparent. A more likely explanation for the unusual behavior of the DW factors regards the FEFF calculation below $k = 3$ $Å^{-1}$. This low k range contains a large percentage of the information about the MS paths. To recover the true MS DW factors, accurate amplitude information is essential in this low k region, but this may be beyond the capabilities of the current versions of the FEFF code.

C. XANES Spectra. Figure 7a shows the normalized XANES region for a 0.145 *m* aqueous chromate solution at a high solution pH, where the CrO_4^{2-} is the dominant species, and for a low solution pH, where the $HCrO_4^-$ and $Cr_2O_7^{2-}$ species dominate. The prominent pre-edge feature near 5994 eV arises

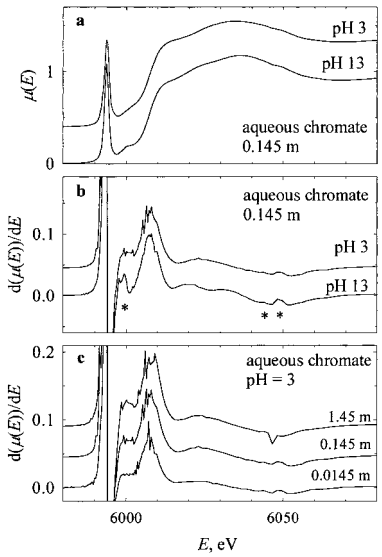

Figure 7. XANES region at the chrome *K* edge of two aqueous chromate solutions at pH 3 and 13 (a) and their first derivatives (b). Asterisks indicate multielectron transitions. The different behavior in the region from 6014 to 6040 eV is in part due to Cr−O′ single scattering paths that are present only in the dichromate structure. This is supported by the maximum near 6022 eV in the derivative spectrum of aqueous chromate solutions at low pH (c) that becomes less intense at lower total chrome concentrations where the bichromate species becomes dominant. The spectra are offset for clarity.

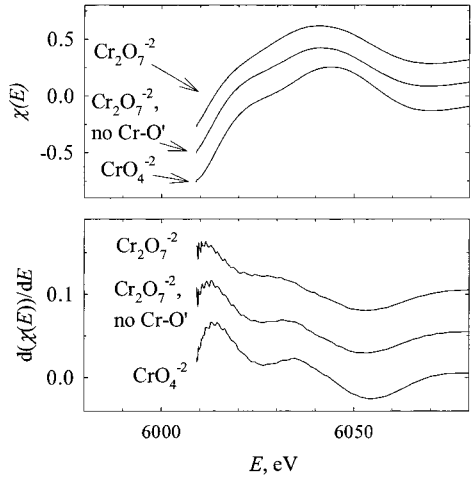

Figure 8. Calculated XANES region (top) and the corresponding derivative (bottom), for a model dichromate molecule, for a model dichromate molecule omitting the Cr−O′ single scattering paths (∼3.7 Å) involving the oxygen atoms of the neighboring CrO'_3, and for a chromate molecule. The significance of the Cr−O′ single scattering contributions is evident.

from the 1s to 3d bound state transition that is highly absorbing in chromium(VI) containing compounds, due to the noncentrosymmetric tetrahedral symmetry that allows for considerable mixing of O(2p) and Cr(3d) orbitals. This effect is well known and has been exploited a number of times to quantitatively analyze the chromium(VI) content in soil,[39,40] lunar samples,[41] in reacting hydrothermal systems,[42] and in surface speciation studies.[43,44]

The derivative spectrum of the XANES region is shown in Figure 7b. The derivative spectrum readily reveals the sharp features near 6000, 6045, and 6050 eV, that have been previously assigned to ($\underline{1s}$, $\underline{t_2}$, t_2^{*2}), ($\underline{1s}$, $\underline{3p}$, t_2^{*2}), and ($\underline{1s}$, $\underline{3p}$, t_2^1, $\epsilon p1$) multielectron transitions (indicated in Figure 7b by asterisks).[45] These multielectron transitions appear to be somewhat less intense in the low-pH XANES spectrum, especially the transitions near 6000 and 6050 eV.

There are two distinct maxima near 6018 and 6032 eV in the derivative of the XANES spectrum at pH 13. Analysis of the various scattering path contributions for the CrO_4^{2-} structure indicated that these arise from the combined contributions of all of the MS paths shown in Figure 5. The derivative of the XANES spectrum at pH 3 shows only one broadly defined maximum near 6022 eV. This broad feature is not captured in the fit to the experimental data using the structural parameters listed in Table 5. To investigate this aspect in more detail, we used the FEFF code to calculate the XANES of an isolated dichromate molecule having atomic coordinates that were the same as those of solid sodium dichromate (all DW factors were set to zero), given by Kharitonov et al.[35] The resulting spectrum with its derivative is shown in Figure 8. These results are compared in Figure 8 with results that were obtained by leaving out the single scattering contributions from Cr with two oxygen atoms (Cr−O′) on the adjoining $-CrO_3$ unit that are at a distance of about 3.7 Å away from the chrome center. Finally, the results of a calculation for the tetrahedral CrO_4^{2-} ion are also included in Figure 8. Although the model calculation for the dichromate ion does not quantitatively reproduce the broad maximum near 6022 eV in the derivative spectrum, the Cr−O′ scattering contribution does qualitatively reproduce this spectral feature. Furthermore, in the experimental data, this spectral feature declines in strength as the total chrome content is lowered, as illustrated in Figure 7c. Since the Cr−O′ path can only be present in the dichromate structure but not in the bichromate structure, the spectral changes in Figure 7c provide further support that the Cr−O′ scattering path contributes to this spectral feature. The Cr−Cr single scattering path contribution could also potentially lead to an XANES peak, but FEFF analysis showed that the amplitudes of this path were too weak in this spectral region.

Encouraged by this finding, we included a Cr−O′ scattering path in the overall fit to the low-pH EXAFS data, by weighting the contributions of this path by the dichromate mole fractions, $x_{Cr,di}$, that were obtained from the IR measurements, as summarized in Table 2. Inclusion of this path slightly improved the fits to the XAFS data, decreasing the fractional misfit R by about 0.002. However, all of the other fitted parameters listed in Table 3 remained essentially unaffected. The average fit results for the Cr−O′ distance and corresponding DW factor were found to be 3.73 ± 0.09 Å and $14.5 \times 10^{-3} \pm 25.5 \times 10^{-3}$ Å^2, respectively.

Judging from the bond distances and angles in the dichromate structure, the $-CrO_3$ units should be free to rotate, and one might therefore expect a larger DW factor for the Cr−O′ path. Although the uncertainties are rather large, the obtained DW factor for this path appears to be relatively small. Furthermore, these values were obtained when the number of Cr−O′ paths was set to two, which would correspond to the eclipsed orientation of the $-CrO_3$ units in the dichromate structure with two short, equivalent Cr−O′ bonds. The same eclipsed structure is also present in the sodium dichromate solid, and the average Cr−O′ bond distance of 3.67 Å found in the solid[35] is very similar to the solution distance of 3.73 Å. It is conceivable that one or more hydrogen-bonded bridging water molecules may hinder a free rotation of the $-CrO_3$ units in the dichromate molecule and may thereby stabilize an eclipsed orientation of the $-CrO_3$ units. It would be interesting to see if there is any evidence of such bridging water molecules in a neutron or X-ray diffraction experiment.

Conclusions

A complete description of the structures and equilibria of the chromate, bichromate, and dichromate species in aqueous solutions was obtained from IR and XAFS spectroscopic investigations. An EXAFS study of low-pH chromate solutions, as a function of total chrome concentration, revealed that the local first-shell oxygen structure around the chrome atom is nearly the same for the bichromate and dichromate species. In particular the chrome−oxygen bond distances to the three terminal oxygen atoms are virtually identical. This structural similarity offers an explanation as to why the $\nu_{as}(CO_3)$ asymmetric stretching band in the IR region is at the same resonance frequency of 949 cm^{-1} for the bi- and dichromate. That this band arises from both species was confirmed by the quantitative analysis of the IR band intensities. Hence, there is conclusive evidence that the previously reported $\nu_s(CO_3)$ symmetric stretching band in the Raman is due to both the bi- and dichromate species. Furthermore, spectral changes observed in the XANES region, combined with the analysis of the EXAFS region suggest that the $-CrO_3$ structural units in the dichromate molecule do not rotate freely but are held in a fixed eclipsed relative orientation, presumably by the presence of stabilizing bridging water molecules. Equilibrium constants that were obtained from the quantitative IR analysis are in good agreement with previously reported values.

Acknowledgment. This research was supported by the Director, Office of Environmental Management Sciences, of the U.S. Department of Energy, under contract DE-AC06-76RLO 1830. We also thank the beamline personnel of the sector ID-20 at the Advanced Photon Source for the assistance that they provided.

References and Notes

(1) Neuss, J. D.; Rieman, W. *J. Am. Chem. Soc.* **1934**, *56*, 2238.
(2) Sasaki, Y. *Acta Chem. Scand.* **1962**, *16*, 719.
(3) Linge, H. G.; Jones, A. L. *Aust. J. Chem.* **1968**, *21*, 1445.
(4) Linge, H. G.; Jones, A. L. *Aust. J. Chem.* **1968**, *21*, 2189.
(5) Haight, G. P., Jr.; Richardson, D. C.; Coburn, N. H. *Inorg. Chem.* **1964**, *3*, 1777−1780.
(6) Palmer, D. A.; Wesolowski, D.; Mesmer, R. E. *J. Solution Chem.* **1987**, *16* (6), 443−463.
(7) Hovey, J. K.; Hepler, L. G. *J. Phys. Chem.* **1990**, *94*, 7821−7834.
(8) Chlistunoff, J. B.; Johnston, K. P. *J. Phys. Chem. B* **1998**, *102*, 3993−4003.
(9) Michel, G.; Cahay, R. *J. Raman Spectrosc.* **1986**, *17*, 79−82.
(10) Michel, G.; Machiroux, R. *J. Raman Spectrosc.* **1983**, *14* (1), 22−27.
(11) Palmer, D. A.; Begun, G. M.; Ward, F. H. *Rev. Sci. Instrum.* **1993**, *64* (7), 1994−1998.
(12) Walrafen, G. E. *J. Chem. Phys.* **1962**, *37*, 662.
(13) Walrafen, G. E. *J. Chem. Phys.* **1963**, *39*, 1479.
(14) Peterson, M. L.; Brown, G. E.; Parks, G. A. *Colloids Surf.* **1996**, *107*, 77−88.
(15) Pandya, K. I. *Physica B* **1994**, *50* (21), 15509−15512.
(16) Darab, J. G.; Li. H.; Matson, D. W.; Smith, P. A.; MacCrone, R. K. In *Synchrotron Radiation Techniques in Industrial Chemical and Materials Science*; D'Amico, K. L., Terminell, L. J., Shuh, D. K., Eds.; Plenum Publishing Co.: New York, 1996; pp 237−255.
(17) Casler, D. G.; Hrma, P. In *Scientific Basis for Nuclear Waste Management XXII*; Wronkiewicz, D. J., Lee, J. H., Eds.; Materials Research Society: Warrendale, PA, 1999; pp 255−262.
(18) Hoffmann, M. M.; Darab, J. G.; Fulton, J. L. *J. Phys. Chem. A*, manuscript submitted.
(19) Hoffmann, M. M.; Addleman, R. S.; Fulton, J. L. *Rev. Sci. Instrum.* **2000**, *71* (3), 1552−1556.
(20) Marquardt, D. W. *J. Soc. Ind. Appl. Math.* **1963**, *11*, 431−441.
(21) Teo, B.-K. *EXAFS, Basic Principles and Data Analysis;* Springer Publishing: New York, 1986.
(22) Koningsberger, D. C.; Prins, R. *X-ray Absorpton: Principles, Applications, Techniques of EXAFS, SEXAFS and XANES;* Wiley: New York, 1988.
(23) Newville, M.; Livins, P.; Yacoby, Y.; Rehr, J. J.; Stern, E. A. *Phys. Rev. B* **1993**, *48*, 14126−14312.
(24) Newville, M.; Ravel, R.; Haskel, D.; Rehr, J. H.; Stern, E. A.; Yacoby, Y. *Physica B* **1995**, *208 & 209*, 154−156.
(25) Zabinsky, S. I.; Rehr, J. J.; Ankudinov, A.; Albers, R. C.; Eller, M. J. *Phys. Rev. B* **1995**, *52*, 2995−3009.
(26) Haskel, D.; Stern, E. A.; Dogan, F.; Moodenbaugh, A. R. *Phys. Rev. B* **2000**, *61* (10), 7055−7076.
(27) Stammreich, H.; Bassi, D.; Sala, O.; Siebert, H. *Spectrochim. Acta* **1958**, *13*, 192−196.
(28) Walrafen, G. E.; Hokmabadi, M. S.; Yang, W.-H. *J. Chem. Phys.* **1986**, *85*, 6964−6969.
(29) Lide, D. R. *CRC Handbook of Chemistry and Physics*, 75th ed.; CRC Press: Boca Raton, FL, 1994.
(30) Tong, J. Y.; Johnson, R. L. *Inorg. Chem.* **1966**, *5*, 1902.
(31) Hobbs, W. E. *J. Chem. Phys.* **1958**, *28*, 1220−1222.
(32) Stammreich, H.; Kawai, K.; Tavares, Y. *Spectrochim. Acta* **1959**, *15*, 438−447.
(33) Nimmo, J. K. *Acta Crystallogr., Sect. B* **1981**, *37*, 431−433.
(34) Ruben, H.; Olovsson I.; Zalkin A.; Templeton, D. H. *Acta Crystallogr., Sect. B* **1973**, *29*, 2963−2964.
(35) Kharitonov, Ju. A.; Kuz'min, E. A.; Belov, N. V. *Kristallografiya* **1970**, *15*, 942−968.
(36) Hoffmann, M. M.; Darab, J. G.; Heald, S. M.; Yonker, C. R.; Fulton, J. L. *Chem. Geol.* **2000**, *167*, 89−103.
(37) Tan, Z.; Budnick, J.; Heald, S. M. *Rev. Sci. Instrum.* **1989**, *60* (6), 1021−1025.
(38) Caminiti, R.; Cilloco, F.; Felici, R. *Mol. Phys.* **1992**, *76* (3), 681−691.
(39) Peterson, M. L.; Brown, G. E., Jr.; Parks, G. A. *Mater. Res. Soc. Symp. Proc.* **1997**, *432*, 75−80.
(40) Szulczewski, M. D.; Helmke, P. A.; Bleam, W. F. *Environ. Sci. Technol.* **1997**, *31*, 2954−2959.
(41) Sutton, S. R.; Jones, K. W.; Gordon, B.; Rivers, M. L.; Bajt S.; Smith, J. V. *Geochim. Cosmochim. Acta* **1993**, *57*, 461−468.
(42) Hoffmann, M. M.; Darab, J. G.; Fulton, J. L. *Proceedings of the 13th International Conference on the Properties of Water and Steam, Toronto, Canada*; NRC Press: Ottawa, 2000.
(43) Peterson, M. L.; Brown, G. E., Jr.; Parks, G. A.; Stein, C. L. *Geochim. Cosmochim. Acta* **1997**, *61*, 3399−3412.
(44) Wainright, J. S.; Murphy, O. J.; Antonio, M. R. *Corros. Sci.* **1991**, *33* (2), 281−293.
(45) Bianconi, A.; Garcia, J.; Benfatto, M.; Marcelli, A.; Natoli, C. R.; Ruiz-Lopez, M. F. *Phys. Rev. B* **1991**, *43* (9), 6885−6892.